

RESEARCH

Open Access



# Bulk RNA-seq conjoined with ScRNA-seq analysis reveals the molecular characteristics of nucleus pulposus cell ferroptosis in rat aging intervertebral discs

Shipeng Chen<sup>1,2†</sup>, Jiawei Fu<sup>1,2†</sup>, Jiang Long<sup>1,2†</sup>, Chang Liu<sup>1,2</sup>, Xuezheng Ai<sup>1,2</sup>, Dan Long<sup>1,2</sup>, Xue Leng<sup>1,2</sup>, Yang Zhang<sup>1,2</sup>, Zhengao Liao<sup>1,2</sup>, Changqing Li<sup>1,2</sup>, Yue Zhou<sup>1,2</sup>, Shiwu Dong<sup>3,4\*</sup>, Bo Huang<sup>1,2\*</sup> and Chencheng Feng<sup>1,2\*</sup>

## Abstract

**Objective** Recently, several studies have reported that nucleus pulposus (NP) cell ferroptosis plays a key role in IDD. However, the characteristics and molecular mechanisms of cell subsets involved remain unclear. We aimed to define the key factors driving ferroptosis, and the characteristics of ferroptotic NP cells subsets during IDD.

**Methods** The accumulation of iron ions in NP tissues of rats caudal intervertebral discs (IVDs) was determined by Prussian blue staining. Fluorescent probe Undecanoyl Boron Dipyrromethene (C11-BODIPY) and lipid peroxidation product 4-Hydroxynonenal (4-HNE) staining were performed to assess lipid peroxidation level of NP cells. The differentially expressed genes in NP tissues with aging were overlapped with FerrDB database to screen ferroptosis driving genes associated with aging-related IDD. In addition, single cell sequencing (ScRNA-seq) was used to map the NP cells, and further identify ferroptotic NP cell subsets, as well as their crucial drivers. Finally, cluster analysis was performed to identify the marker genes of ferroptotic NP cells.

**Results** Histological staining showed that, compared with 10 months old (10M-old) group, the accumulation of iron ions increased in NP tissues of 20 months old (20M-old) rats, and the level of lipid peroxidation was also enhanced. 15 ferroptosis driving factors related to IDD were selected by cross-enrichment. ScRNA-seq identified 14 subsets in NP tissue cells, among which the number and ratio of 5 subsets was reduced, and the intracellular ferroptosis related signaling pathways were significantly enriched, accompanied by enhanced cell lipid peroxidation. Notably, ranking the up-regulation fold of ferroptosis related genes, we found Atf3 was always present within TOP2 of these five cell subsets, suggests it is the key driving factor in NP cell ferroptosis. Finally, cluster cross-enrichment and fluorescence colocalization analysis revealed that Rps6 +/Cxcl1- was a common molecular feature among the 5 ferroptotic NP cell subsets.

<sup>†</sup>Shipeng Chen, Jiawei Fu and Jiang Long contributed equally to this work.

\*Correspondence:

Shiwu Dong

dongshiwu@163.com

Bo Huang

fmmu@126.com

Chencheng Feng

doctorfgy@tmmu.edu.cn; doctorfgy@163.com

Full list of author information is available at the end of the article



**Conclusions** This study reveals that ATF3 is a key driver of NP cell ferroptosis during IDD, and Rps6 +/Cxcl1- is a common molecular feature of ferroptotic NP cell subsets. These findings provide evidence and theoretical support for subsequent targeted intervention of NP cell ferroptosis, as well as provide directions for preventing and delaying IDD.

**Keywords** IDD, NP cells, ScRNA-seq, Ferroptosis, Atf3, Rps6 +/Cxcl1

## Introduction

Low back pain (LBP) is a global musculoskeletal disease that has significant influence on the quality of life [1–3]. Intervertebral disc degeneration (IDD) is the main cause of LBP and has been shown to be closely related to aging [4, 5]. Physiologically, intervertebral disc (IVD) is a special organ composed of endplate, annulus fibrosus, and nucleus pulposus (NP) that connects vertebrae. With aging, degenerative discs are characteristic with stromal fibrosis, cell death and excessive release of inflammatory factors, and these changes exacerbate the IVDs degradation [6–8]. NP plays a central role in the homeostasis of IVDs, and is responsible for maintaining IVDs height, supporting body weight and buffering external forces [9, 10]. Numerous studies have shown that degenerative NP tissues are characteristic with reduction of functional NP cells. During IDD, NP cells undergo cell cycle arrest, cell death, oxidative stress and secretion of inflammatory factors and matrix catabolic enzymes, which further affect the fate of neighboring normal cell [4, 11, 12]. Therefore, further exploration of the key mechanisms causing NP cell death and number reduction is of great significance for alleviating or delaying IDD.

In recent years, more and more studies have demonstrated that NP cell ferroptosis is involved in the aging-related IDD [13, 14]. Ferroptosis is a novel type of programmed cell death first proposed by Dixon et al., in 2012 [15]. Ferroptosis is lipid peroxidation induced by iron overload, and its excessive accumulation will cause cell membrane damage and lead to cell death [16]. Aberrant activation of genes related to lipid synthesis and oxidative is an important driver of ferroptosis. Acyl-CoA synthase long chain family member 4 (Acsl4) and lysophosphatidylcholine acyltransferase 3 (Lpcat3) are responsible for catalyzing and integrating polyunsaturated fatty acids (PUFA) into membrane phospholipids (PL). The peroxidation of PUFA bound to the cell membrane will directly lead to cell ferroptosis [17, 18]. Besides, the imbalance of amino acid antioxidant system is another important mechanism causing cell ferroptosis. The glutamate-cystine reverse transport system Xc<sup>-</sup> is composed of solute transport families 7A11 (SLC7A11) and SLC3A2, and exchanges intracellular glutamate for extracellular cystine in a ratio of 1:1, thereby synthesizing GSH, the main antioxidant in cells [19, 20]. Inhibition of any component of system Xc<sup>-</sup> disrupts cystine

uptake and induces ferroptosis [21, 22]. Although abnormal expression of ferroptosis related genes and enrichment of ferroptosis related signaling pathways have been identified in aging NP cells, the molecular features of ferroptotic NP cells and specific cell clusters targeted by ferroptosis in IDD remain largely unknown [23]. Therefore, a deeper understanding of the characteristics and mechanisms of NP cell ferroptosis will help to identify its intrinsic pathogenic factors and provide new therapeutic targets for IDD.

With the development of high-throughput sequencing technology, the comprehensive understanding of transcriptomic characteristics of NP tissues and the identification of specific NP cell subsets have made a great breakthrough [24, 25]. In our previous series of studies, we found widespread cell death, decreased number and enhanced oxidative stress in aged rat NP cells, which may be closely related to NP cell ferroptosis [26–28]. Furthermore, compared with other animal IDD models (such as mice, goats and cattle), rat model has many advantages, including convenient sampling, shorter life cycle, moderate volume of NP tissues. To obtain a comprehensive cellular map of rat IVD NP tissues, further determine the role and characteristics of NP cell ferroptosis in IDD, we investigate the key factors driving ferroptosis of NP cells during aging-related IDD of rats based on conjoint analysis of single cell sequencing (ScRNA-seq) and RNA sequencing of bulk samples (Bulk RNA-seq). At the same time, we also analyzed and identified the expression biomarkers of NP cell subsets undergoing ferroptosis, which contributes to further understanding of the molecular mechanism of NP cell ferroptosis in the process of IDD, and to determining the potential specific targeted cells and signaling molecules for intervention.

## Materials and methods

### Animals

All male Sprague–Dawley (SD) rats (10M-old:  $n = 11$ ; 20M-old:  $n = 11$ ) were obtained from the Animal Center of Second Affiliated Hospital, Army Medical University, Chongqing, China. All experimental procedures were approved by the hospital Animal Ethics Committee (Registration approval number: AMUWEC2020088). The animals were housed under specific pathogen-free (SPF) conditions at approximately 25 °C and 50% humidity, with a 12-h light/dark cycle, and fed ad libitum.

### Rat IVDs and NP tissues harvest

Male SD rats with two ages were classified into two groups: 10M-old group ( $450 \pm 45$  g,  $n = 11$ ) and 20M-old group ( $750 \pm 75$  g,  $n = 11$ ) (A total of 6 SD rats from both groups were used for histopathological evaluation and 8 rats were used for primary cell extraction. The remaining 8 SD rats were treated with ScRNA-seq). The tail IVDs (Co3/4,  $n = 3$ ) of 6 rats were obtained, and the 10  $\mu$ m axial cryosections of disc were obtained from its transverse section. Then, the tail IVDs (Co4/5,  $n = 3$ ) were obtained for paraffin embedding, sectionalization, and subsequent histological analysis. In addition, NP tissue from all tail IVDs of 8 rats was obtained for primary cell extraction. All tail IVD NP tissues from the remaining 8 rats were used for ScRNA-seq.

The NP tissues were harvested as follows: First, rats were anesthetized with sodium pentobarbital (0.2%, 0.3 mL/100 g) and euthanized by cervical dislocation. Next, the tails were routinely disinfected, and the skin and subcutaneous tissue were incised along the posterior midline. Muscles, tendons and ligaments were bluntly separated with hemostatic forceps to expose IVDs. Finally, an incision was made at the annulus fibrosus to obtain milky NP tissue.

### Prussian blue staining of rat IVD NP tissue

The caudal IVDs of rat ( $n = 3$ ) were fixed in 4% paraformaldehyde (PFA) and decalcified for 2 weeks at 37 °C in 10% EDTA decalcification solution. Afterwards, the discs were embedded in paraffin and sectioned into 5  $\mu$ m slices for subsequent histological staining. According to the manufacturer's program, the paraffin sections were stained with Prussian blue (3,3'-Diaminobenzidine, DAB) dye kits (Hubei BIOS Biotechnology Co., LTD.) to assess iron ion metabolism. Specifically, (1) the slices were routinely dewaxed and rehydrated. (2) Perls stain working solution (37°C, 20 min) was added in drops, and then washed 3 times with distilled water. (3) The incubation solution was added (37°C, 10 - 20 min), and then the solution was soaked with PBS for 3 times. (4) The enhanced working solution was added by dropping (37°C, 10 - 20 min), and then soak with PBS for 3 times. (5) The dye was stained by dropping the compound solution for 3 - 5 min, and then soaked with distilled water for 10 min. Finally, dehydration and sealing are carried out.

### Immunofluorescence staining

The frozen sections ( $n = 3$ ) were rewarmed at room temperature for 15 min. Then the membrane was broken with 0.1% cell permeabilization wash buffer (Triton X- 100:PBS = 1000:1) for 15 min. Frozen section antigen repair solution (Solarbio#C1035) was used to repair

for 10 min. The slices were sealed and overnight at 4 °C with a primary antibody, including 4-HNE (Abcam, No: ab46545, 1 mg/mL, dilution: 1:1000), ACSL4 (Abcam, No: ab155282, 1 mg/mL, dilution: 1:200), Atf3 (ThermoFisher, No: PA5 - 106898, 1 mg/mL, dilution: 1:200), Cxcl1 (Affinity Biosciences, No: AF5403, 1 mg/mL, dilution: 1:500) and Rps6 (Bioss, No: bsm- 51406M, 1 mg/mL, dilution: 1:200). The next day, sections were incubated with fluorescently labeled secondary antibodies (DyLight 488, 594 or 555) for 2 h at room temperature in the dark. The cell nuclei were re-stained with DAPI (C1002, Beyotime, China), and the staining was observed by fluorescence microscopy. Additionally, for C11-BodiPY (581/591) staining, the frozen slices rewarmed at room temperature were directly added with 50  $\mu$ l C11-BodiPY dye solution (ThermoFisher #D3861) and incubated at 37 °C for 45 min. The samples were soaked with TBST 3 times for 5 min each time. Then 50  $\mu$ l DAPI working solution (1  $\mu$ g/mL) was added to stain the nucleus for 10 min. Finally, fluorescence intensity was observed by confocal microscopy (LSM 880, Carl Zeiss AG, Germany; Resolution: XY 120nm, Z 500nm).

### Conjoint analysis

Two hundred sixty-four ferroptosis inducers were obtained from the FerrDb V2 database (<http://www.zhounan.org/ferrdb/>). In addition, differentially expressed genes (DEGs) of mRNA-seq were also obtained. Next, an overlapping analysis was performed between selected gene sets from the FerrDb V2 database and DEGs to obtain ferroptosis related genes that play a role in the IDD. To explore the key ferroptosis genes in IDD, we further analyzed the expression of overlapped genes in subsequent single-cell subsets and ranked their fold difference.

### Preparation of NP single-cell suspension

NP tissues of all tail IVDs were collected from a total of 10 rats in 10M-old ( $n = 5$ ) and 20M-old ( $n = 5$ ) groups for single-cell suspension. NP tissues were harvested as described in 2.2 and were washed with phosphate buffer solution (PBS) to remove surface blood clots, and other attachments, and chopped into small pieces. The washed tissue pieces were added with 2 mL type II collagenase (0.2%), gently shaken, digested at 37 °C for 1 h, then filtered through a 70  $\mu$ m cell filter, and centrifuged for 5 min (300 g, 4 °C). The precipitated cells were re-suspended in the red cell lysis buffer for 5 min, then filtered again through a 40  $\mu$ m filter and centrifuged to remove the lysed red cells. The suspension was resuspended in 100  $\mu$ l Dead Cell Removal MicroBeads (MACS 130-090-101) and remove dead cells using Miltenyi® Dead Cell Removal Kit (MACS 130-090-101). Then, the remaining

cells were centrifuged to remove the reagents. After washing with PBS containing 0.04% BSA twice, the cell precipitates were re-suspended.

#### Single cell-seq and library construction

The NP cell suspension was loaded into the 10 × Chromium instrument, cell capture, cDNA amplification and library construction were performed according to the official library kit instructions (10X Genomics Chromium Single-Cell 3' kit, V3). Then, the NovaSeq 6000 sequencing platform was used for sequencing (paired-end multiplexing run, 150 bp). The above technology is provided by Hangzhou Lianchuan (LC-Bio Technology co.ltd., HangZhou, China).

#### Processing of scRNA sequencing data

Sequencing data were parsed and converted to fastq format files using Illumina bcl2 fastq software (version 2.20). Then, data quality statistics were performed on the raw sequencing data of each sample using Cell Ranger, the official analysis software of 10 × Genomics (<https://support.10xgenomics.com/single-cell-geneexpression/software/pipelines/latest/what-is-cell-ranger,version3.1.0>), and the reference genome was aligned. The analysis results showed that a total of 17,064 cells were captured from 10 and 20-month-old NP samples. The analysis result of Cell Ranger is imported into Seurat software (version 3.1.1) for data dimensionization reduction, cluster analysis, and expression matrix analysis. The threshold of quality control conditions is (1) all genes are expressed in at least 3 cells, (2) the number of genes expressed in a single cell is between 500 and 5000, (3) the number of UMI  $\geq$  500, and (4) the ratio of mitochondrial gene expression is less than 25%.

#### Rat NP cell culture

The obtained rat NP tissues were cut into small pieces and added with 2 mL type II collagenase (0.2%), gently shaken, digested at 37 °C for 1 h. Then, it was filtered through a 70µm filter, and NP cells were collected. Rat NP cells were suspended in DMEM/F-12 (01-172 -1 ACS, BI, USA) containing 20% fetal bovine serum (S711 -001 S, Lonsera, Uruguay), 100 units/mL penicillin and 100 µg/mL streptomycin, spread in T25 culture flasks, and cultured at 5% CO<sub>2</sub> and 37 °C.

#### Establishment of NP cell ferroptosis

The ferroptosis of NP cells was induced by erastin. According to the reagent manufacturer's instructions, erastin was dissolved with Dimethyl sulfoxide (DMSO) and incubated in cultured NP cells at a final concentration of 5 µmol/mL for 24 h. Besides, PBS and DMSO were added to the remaining two groups of NP cells as

the blank and control group. Then the effect of ferroptosis was detected by CCK8, Real-time PCR and flow cytometry.

#### Real-time fluorescence quantitative PCR (RT-qPCR)

Total RNA from NP cells was extracted with TriZol reagent (Invitrogen), and the quality and concentration of extracted RNA were determined with NanoDrop ND-1000 spectrophotometer (Thermo Scientific, USA). PrimeScript RT-PCR kit (Takara) was used to synthesize cDNA. Finally, the RT-qPCR system (Thermo Fisher) was used to detect mRNA expression of target genes (Working conditions: 95 °C for 30 s, followed by 40 cycles of 95 °C for 5 s and 60 °C for 30 s, with GAPDH as the endogenous control. The primer sequences for the target genes are as follows: Atf3: forward: 5'-agg tgg ccc ctg aag aag at-3', reverse: 5'-ttg ttt cga cac ttg gca gc-3'; Rps6: forward: 5'-taa aca aag aag gta aga agc cca g-3', reverse: 5'-cgt cgg cgt ttg tgt tg-3'; Cxcl1: forward: 5'-act caa gaa tgg tgc cga gg-3', reverse: 5'-ctt ggg gac acc ctt tag ca-3'.

#### Cell viability quantification

The primary NP cells cultured above were prepared into cell suspension, inoculated into 96-well plates (100 µL/well), and the plates were pre-cultured in an incubator for 24 h. Then 10 µL of Cell Counting Kit-8 (CCK-8) solution was added to each well and incubated in an incubator at 5% CO<sub>2</sub> and 37 °C for 3 h. Finally, the absorbance at 450 nm was measured by Microplate reader (SpectraMax M2), and the cell activity was calculated according to [(Erastin group—blank group)/(DMSO group—blank group)] × 100%.

#### C11-BODIPY flow staining analysis of NP cells

The primary NP cells cultured in erastin treatment group, control (DMSO) group and blank group were digested and washed, and transferred to 1.5 mL brown dark EP tubes. Then, centrifuge to discard the supernatant. 1 mL of 1 µg/mL C11-BODIPY staining solution was added to each tube and stained for 15 min at room temperature in the dark. After centrifugation, the supernatant was discarded, and the cells were re-suspended with PBS and cleaned 2 to 3 times, and finally the cells were re-suspended with 400 µL PBS. The treated cells were subjected to flow cytometry analysis. Finally, data were imported into Summit software, the gating conditions were set, the target cell population was selected, and the fluorescence intensity between the groups was compared to analyze the lipid peroxidation level of NP cells.

#### Statistical analysis

All experiments were independently performed at least three times, and the GraphPad Prism software was used

for statistical analysis. Normal distribution of the data was assessed through Shapiro–Wilk test. In addition, the non-normally distributed data is logarithmically converted to normally distributed data. The measured data are presented as mean  $\pm$  standard deviation. Differences between two groups of normally distributed data were compared by Student's *t* test, and the differences between groups were compared using one-way ANOVA.  $P < 0.05$  was considered statistically significant.

## Results

### NP cell ferroptosis in aging-related IDD

According to our previous studies, we analyzed three age groups of IVDs in humans (youth, middle age and elderly group) and rats (2, 10 and 20 months old), and found that IVDs showed aging-related degeneration. Notably, compared with the stage from 2 to 10 months old, the differences in cell death and oxidative stress levels were more significant in rats IDD from 10 to 20 months old [27, 28]. In this study, we further investigated the molecular features of NP cell ferroptosis during rats IDD from 10 to 20 months old. The research methodology employed is illustrated in the graphical flow chart (Fig. 1). Prussian blue staining showed the increased accumulation of iron ions in outer annulus fibrosus (OAF), internal annulus fibrosus (IAF), and NP tissues in the 20 months old (20M-old) group. (Fig. 2A). In addition, C11-BODIPY staining showed that lipid peroxidation levels were increased in

OAF, IAF and NP tissue cells (Fig. 2B–C), and the expression of lipid peroxidation product 4-hydroxynonenal (4-HNE) was also up-regulated (Fig. 2D–E). Especially in NP cells of degenerative IVDs, the differences in ferroptosis related indicators were more pronounced (Fig. 2B–E), suggesting the occurrence of cell ferroptosis during the process of IDD.

To determine whether there are aging-related changes in NP cells during IDD, we compared 10 and 20 months old NP RNA-seq data obtained from our previous studies (Expression Omnibus database (<https://www.ncbi.nlm.nih.gov/>) GSE234369) [29]. The results showed that, compared with the 10 months old (10M-old), 307 genes were significantly up-regulated and 650 genes were dramatically down-regulated in the 20M-old group (Fig. 2F). Gene Ontology (GO) analysis showed that the up-regulated genes were mainly enriched in extracellular matrix, oxygen transport and negative regulation of angiogenesis (Fig. 2G). The down-regulated genes were mainly involved in double-strand break repair, vitamin transport and negative regulation of hormone metabolic process (Fig. 2H). In addition, Kyoto Encyclopedia of Genes and Genomes (KEGG) analysis showed that up-regulated genes were mainly enriched in TGF- $\beta$  signaling pathway, FoxO signaling pathway and Relaxin signaling pathway (Fig. 2I). The down-regulated genes were mainly related to the mTOR signaling pathway, biosynthesis of cofactors and circadian rhythm (Fig. 2J). These enriched entries

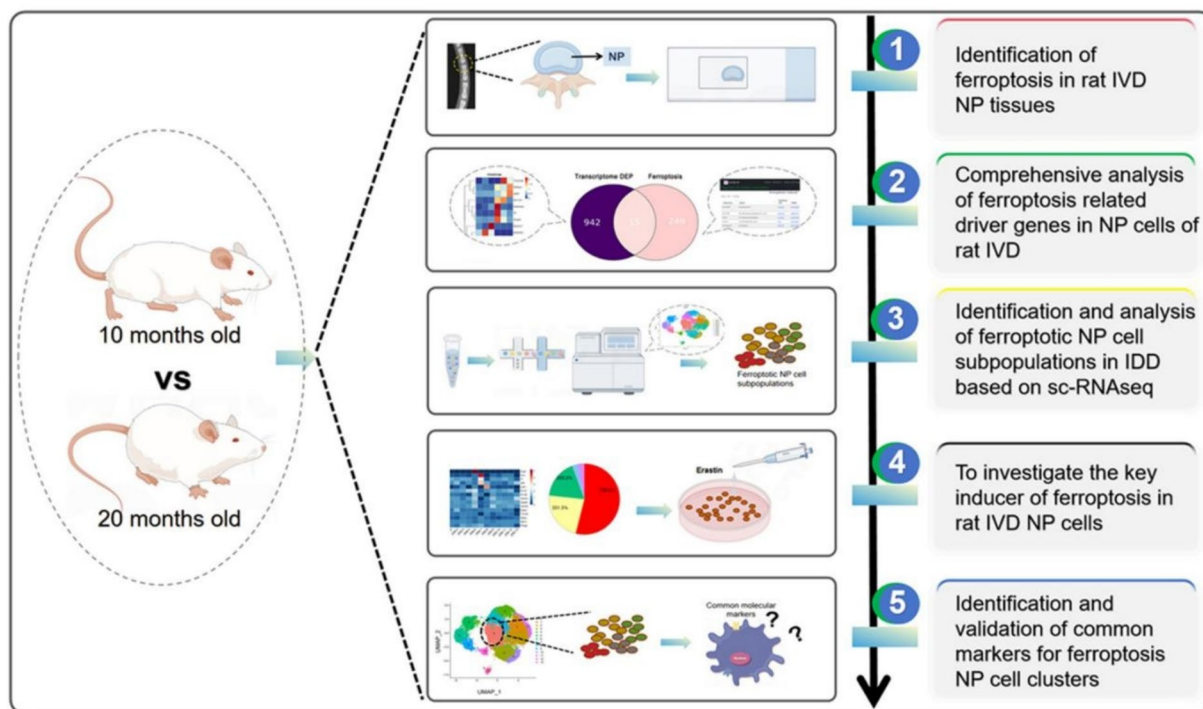


**Fig. 1** Flowchart of the whole study

are intrinsic characteristics of cellular aging. Based on the above results, it shows that ferroptosis of NP cells is closely related to the occurrence and development of aging-related IDD.

### Comprehensive analysis of ferroptosis related driver genes of NP cells

To explore these regulators that contribute to the ferroptosis of NP cells during IDD, we obtained 264 ferroptosis related drivers from FerrDb V2 database, and then overlapped them with the DEGs of NP tissues with aging. As a result, 15 ferroptosis drivers associated with the development of IDD were obtained (Fig. 3A), and the details are shown in Table 1. The expression changes of these 15 ferroptosis-related genes were further analyzed based on the RNA-seq data of NP tissues. Compared with the 10M-old, 7 genes were up-regulated and 8 genes were down-regulated in the 20M-old group (Fig. 3B). Pearson correlation analysis showed that the 15 ferroptosis-related genes were associated with each other (Fig. 3C). Furthermore, GO analysis showed that these genes were mainly enriched in cell differentiation, cell proliferation and apoptosis, lipid metabolism, glycogen synthesis and other biological processes; cell components including cell membrane, mitochondria and its outer membrane (Fig. 3D). KEGG analysis showed that the 15 ferroptosis-related genes of NP cells were mainly enriched in insulin signaling pathway, mTOR signaling pathway, PI3 K-Akt signaling pathway, ferroptosis and hedgehog signaling pathway (Fig. 3E). These enriched terms are closely related to aging and IDD [28, 30–32], which demonstrated that these 15 genes are involved in regulating ferroptosis in NP cells of aging IVDs.

### The changes of NP cell subpopulations during aging-related IDD

In order to investigate NP cell subpopulations during IDD, we performed ScRNA-seq of rat NP cells. The schematic workflow of NP cell ScRNA-seq was shown in Fig. 4A. After the initial quality control assessment, we

obtained a total of 17,064 effective cells from both groups (Fig. 4B). According to the transcriptomic characteristics of each cell subpopulation, it was divided into 14 major cell clusters (Fig. 4C). Dimensionality reduction cluster analysis showed that although the rat NP cells from two groups were composed of the same cell types, the UMAP plot of each subpopulation in the two groups showed significant differences (Fig. 4D). It has been reported that NP tissue cells are composed of notochordal NP cells and chondrocyte-like NP cells in IVDs [33]. As the precursor NP progenitor cells of all cells in mature IVD NP, notochordal NP cells enable NP tissues to maintain its ability of multipotency differentiation and self-renewal [34, 35]. We first identified the cluster 13 as notochordal NP cells by the reported marker genes *Krt8* and *Stmn2* [36, 37], and *Krt7* is a newly identified notochordal NP cell marker in this study (Fig. 4E–F). Additionally, chondrocyte-like NP cells are mature functional cells in NP tissues, and they are also the direct executor of various biological functions. According to different biological functions, chondrocyte-like NP cells can be divided into effector, stromal, regulatory and homeostasis NP cells, etc., which together coordinate and maintain IVDs homeostasis and have been widely reported [38, 39]. Here, we analyzed the changes in the proportion of notochordal NP cells and all subsets of mature functional NP cells in aging-associated IDD. Specifically, compared with the 10M-old group, the cell proportion of cluster 1, 2, 3, 5, 6, 9, 10, 11 and 12 in the 20M-old group was markedly increased, while the proportion of cluster 0, 4, 7, 8 and 13 was significantly decreased (Fig. 4G).

### Identification and analysis of ferroptotic NP cell subpopulations during IDD

Ferroptosis is a programmed cell death characterized by iron-dependent lipid peroxidation [40]. To identify the specific subpopulations of NP cells undergoing ferroptosis during IDD, we focused on the clusters with a significant reduction in cell number demonstrated by dimensionality reduction clustering, including cluster 0,

(See figure on next page.)

**Fig. 2** NP cells ferroptosis increased during rats IDD. **A** Prussian blue staining of 10 and 20M-old rat tail IVD sections, with magnified representative images of IAF, OAF, and NP tissue cells at right. Scale bars, 50  $\mu$ m.  $n = 3$ . **B–C** C11-BODIPY staining of IVD cross sections from 10 and 20M-old rat tails, the representative images of enlarged IAF, OAF, and NP tissue cells are shown on the right. Scale bars, 50  $\mu$ m (**B**). The red for unoxidized lipids and green fluorescence for oxidized lipids were conducted quantitative statistical analysis (**C**). Data are expressed as the mean  $\pm$  SEM ( $n = 3$ ). **D–E** Immunofluorescence staining of 4-HNE in IVD transverse sections of 10 and 20M-old rat tails. Representative images of enlarged IAF, OAF, and NP tissue cells are shown on the right. Scale bars, 50  $\mu$ m (**D**). The mean fluorescence intensity of 4-HNE was quantified (**E**). Data are expressed as the mean  $\pm$  SEM ( $n = 3$ ). **F** Bulk RNA-seq of 10 and 20M-old rat NP tissues were obtained from previous studies [29], and the volcano plot was drawn according to the differentially expressed genes (DEGs) during IDD (20 vs 10M-old,  $n = 3$ ). **G–H** The top 10 enriched GO terms that express significantly up-regulated (**G**) and down-regulated (**H**) genes, including three aspects: biological process (BP), cellular component (CC), and molecular function (MF). **(I–J)** The top 10 enriched pathways of genes with significantly up-regulated (**I**) and down-regulated (**J**) expression.

\* $P < 0.05$ , \*\* $P < 0.01$

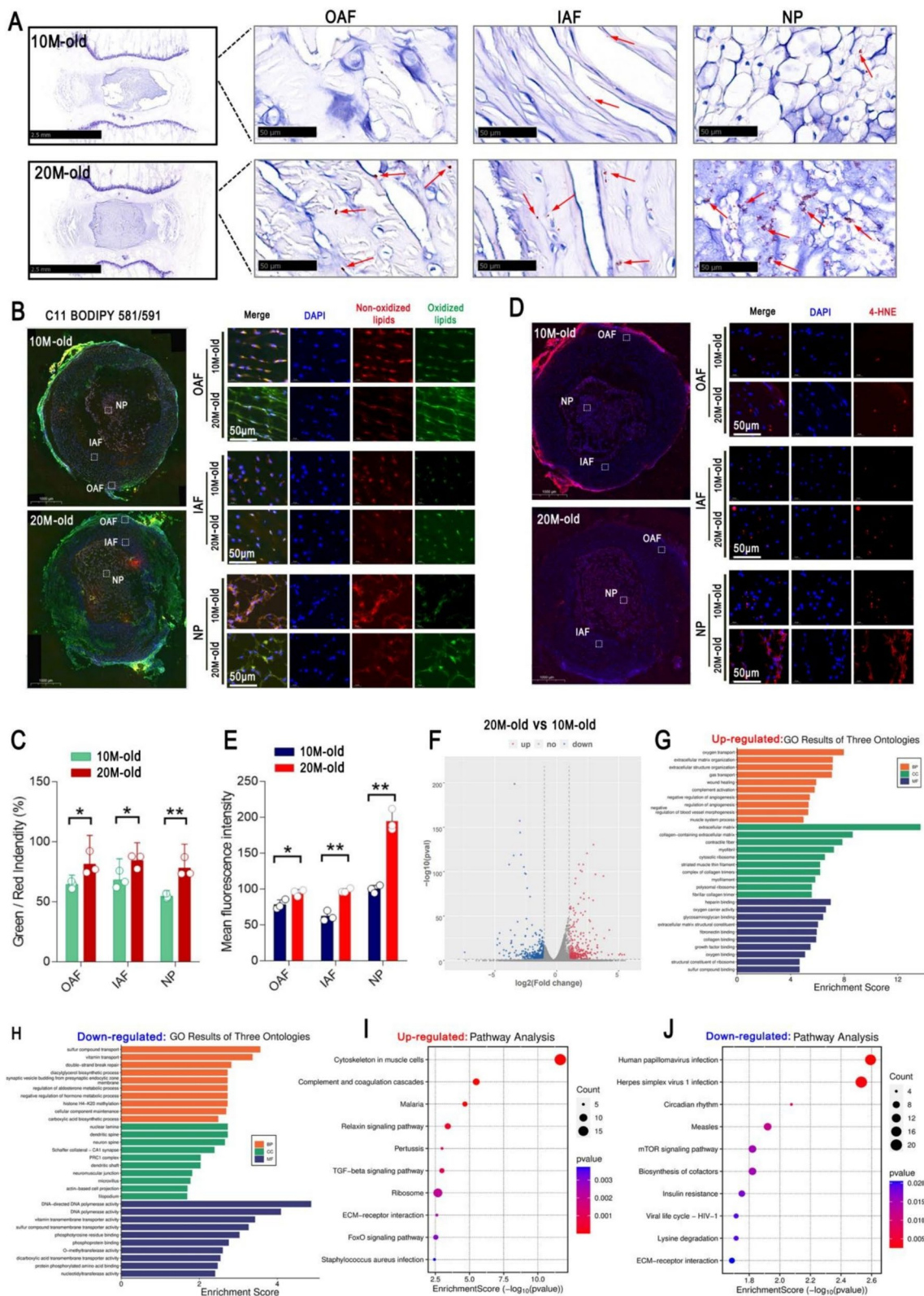


**Fig. 2** (See legend on previous page.)

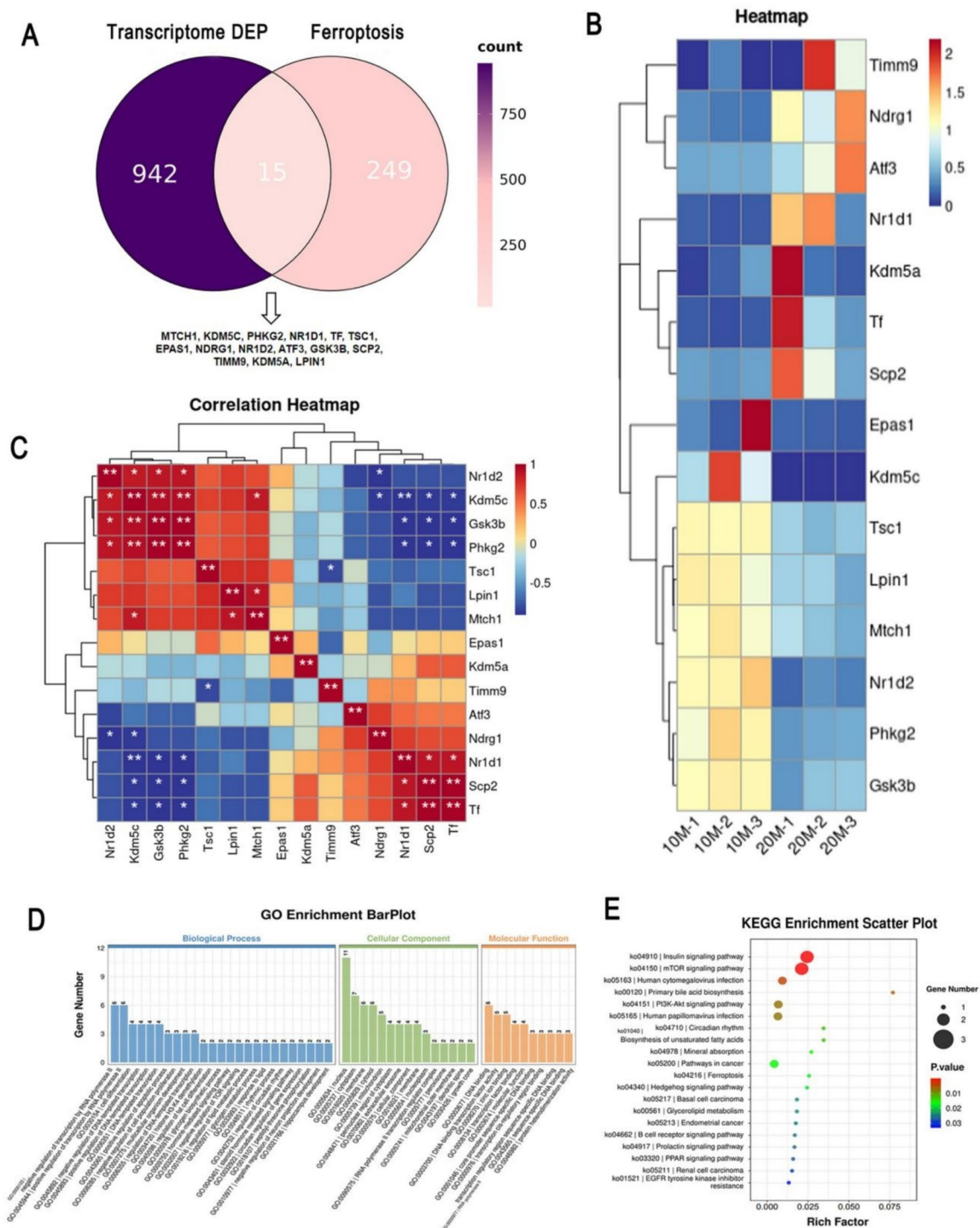


**Fig. 3** Fifteen ferroptosis related genes play a broad regulatory role in NP cells during rats IDD. **A** The DEGs in NP cells of rat IDD were cross-enriched with ferroptosis drivers in the FerrDb database, and 15 ferroptosis-related genes were obtained. **B** The heatmap of 15 ferroptosis-related genes expression in rat NP cells. **C** Pair-wise Pearson correlation heatmap shows the associations between 15 ferroptosis genes. **D** GO analysis of 15 ferroptosis-related genes. **E** KEGG enrichment analysis of 15 ferroptosis related genes

**Table 1** Details of 15 ferroptosis related genes in rat IVD obtained from NCBI

Gene	Description	Location	Summary
Mtch1	Mitochondrial carrier 1	Chromosome 20, NC_086038.1 (7391558..7415291)	Predicted to be involved in activation of cysteine-type endopeptidase activity involved in apoptotic process and positive regulation of apoptotic process
Kdm5c	Lysine demethylase 5C	Chromosome X, NC_086039.1 (24821568..24866423)	Predicted to enable histone H3-methyl-lysine-4 demethylase activity and zinc ion binding activity
Phkg2	Phosphorylase kinase catalytic subunit gamma 2	Chromosome 1, NC_086019.1 (191614738..191627615)	Phosphorylase kinase is a polymer of 16 subunits, four each of alpha, beta, gamma and delta
Nr1 d1	Nuclear receptor subfamily 1, group D, member 1	Chromosome 10, NC_086028.1 (84224599..84231812)	The encoded protein is a ligand-sensitive transcription factor that negatively regulates the expression of core clock proteins
Tf	Transferrin	Chromosome 8, NC_086026.1 (112668667..112695376)	Enables ferric iron binding activity
Tsc1	TSC complex subunit 1	Chromosome 3, NC_086021.1 (32367434..32416565)	Enables GTPase activating protein binding activity and protein N-terminus binding activity
Epas1	Endothelial PAS domain protein 1	Chromosome 6, NC_086024.1 (13543252..13626147)	Enables DNA-binding transcription factor activity and cobalt ion binding activity
Ndrp1	N-myc downstream regulated 1	Chromosome 7, NC_086025.1 (100573526..100614902)	Predicted to enable cadherin binding activity; small GTPase binding activity; and tubulin binding activity
Nr1 d2	Nuclear receptor subfamily 1, group D, member 2	Chromosome 15, NC_086033.1 (9955034..9981329)	The encoded protein functions as a transcriptional repressor and may play a role in circadian rhythms and carbohydrate and lipid metabolism
Atf3	Activating transcription factor 3	Chromosome 13, NC_086031.1 (105274103..105331653)	Enables DNA-binding transcription activator activity, RNA polymerase II-specific and RNA polymerase II transcription regulatory region sequence-specific DNA binding activity
Gsk3b	Glycogen synthase kinase 3 beta	Chromosome 11, NC_086029.1 (76004502..76154665)	Enables several functions, including ATP binding activity; protein kinase activity; and signaling receptor binding activity
Scp2 d1	SCP2 sterol-binding domain containing 1	Chromosome 3, NC_086021.1 (152655282..152656032)	Enables several functions, including ATP binding activity; protein kinase activity; and signaling receptor binding activity
Timm9	Translocase of inner mitochondrial membrane 9	Chromosome 6, NC_086024.1 (95346065..95358895)	Predicted to enable chaperone binding activity; membrane insertase activity; and protein homodimerization activity
Kdm5a	Lysine demethylase 5A	Chromosome 4, NC_086022.1 (155238124..155316121)	Predicted to enable several functions, including DNA binding activity; histone H3-tri/di/monomethyl-lysine-4 demethylase activity; and zinc ion binding activity
Lpin1	Lipin 1	Chromosome 6, NC_086024.1 (45039110..45145845)	Predicted to enable several functions, including histone deacetylase binding activity; peroxisome proliferator activated receptor binding activity; and phosphatidate phosphatase activity

4, 7, 8 and 13 in the 20M-old group (Fig. 5A). GO analysis showed the enrichment of ferroptosis pathway in the top 14 biological processes in these five clusters (Fig. 5B). Moreover, the abnormalities of iron ion metabolism, system Xc- and lipid metabolism are typical features of ferroptosis [41–43]. Thus, we further analyzed the expression of key genes involved in these three typical biological processes in the 5 clusters. Analysis results showed

that, compared with the 10M-old, transferrin receptor protein 1 (Tfrc/Tfr1), as the most important membrane protein regulating intracellular iron transport, was abnormally up-regulated in the 20M-old group, although it was generally less expressed in NP cells (Fig. 5C). The deficiency of the mitochondrial protein frataxin (Fxn), which is involved in the synthesis of iron-sulfur clusters, further leads to an imbalance of intracellular iron

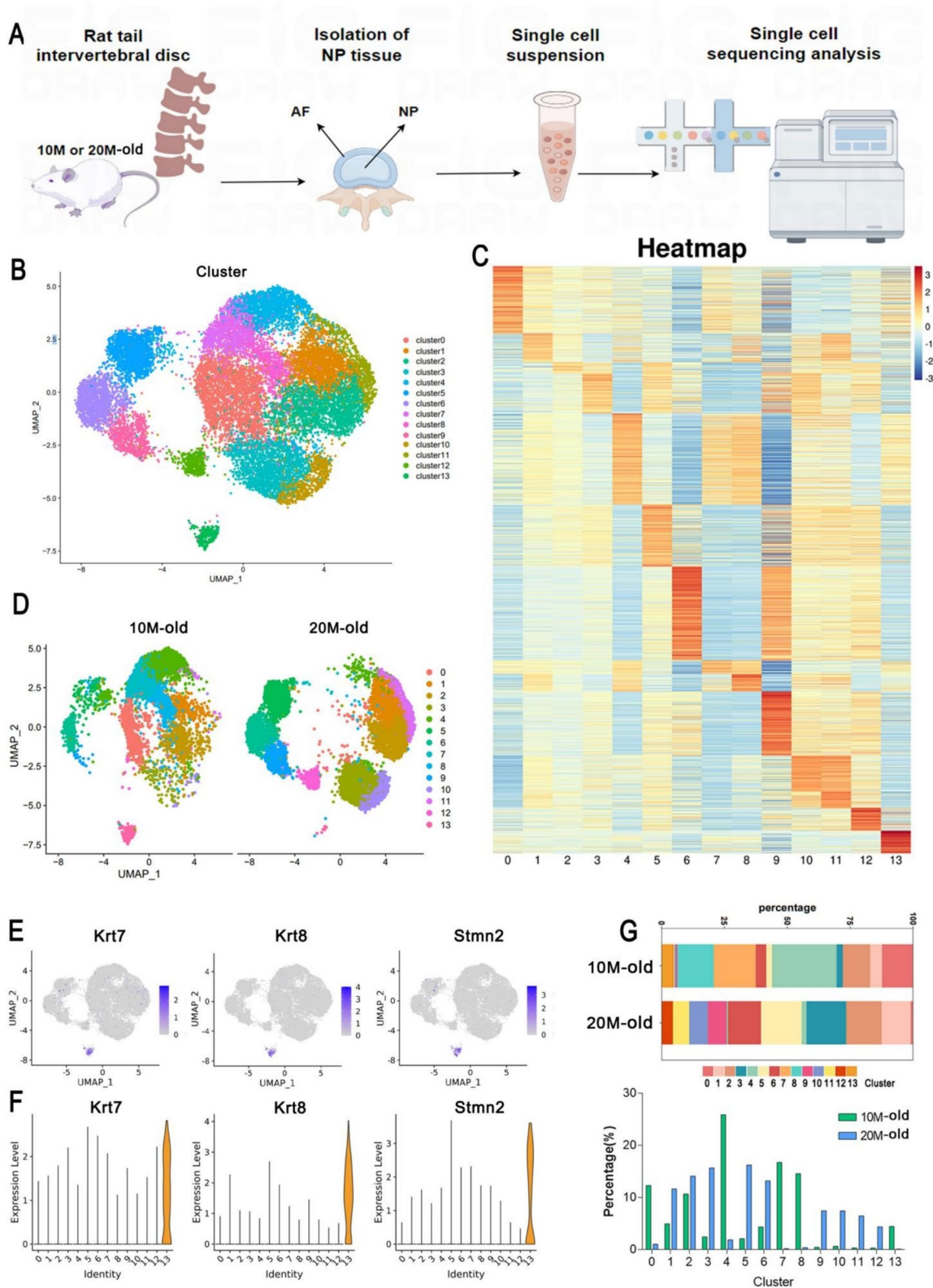


**Fig. 4** Single-cell profiling identifies significant changes in the NP cell profile of degraded IVDs. **A** The processing and analysis workflow of rat IVD NP cells for ScrNA-seq. **B** UMAP plot of total rat IVD NP cells. **C** 14 cell types were identified based on the different transcriptomes of rat IVD NP cells. **D** UMAP plot of NP cells from 10 and 20M-old rats. **E-F** UMAP (E) and violin map (F) of Krt7, Krt8 and Stmn2 expression in the cluster 13 NP cells. **G** The proportion of 14 cell clusters in 10 and 20M-old rat NP tissues

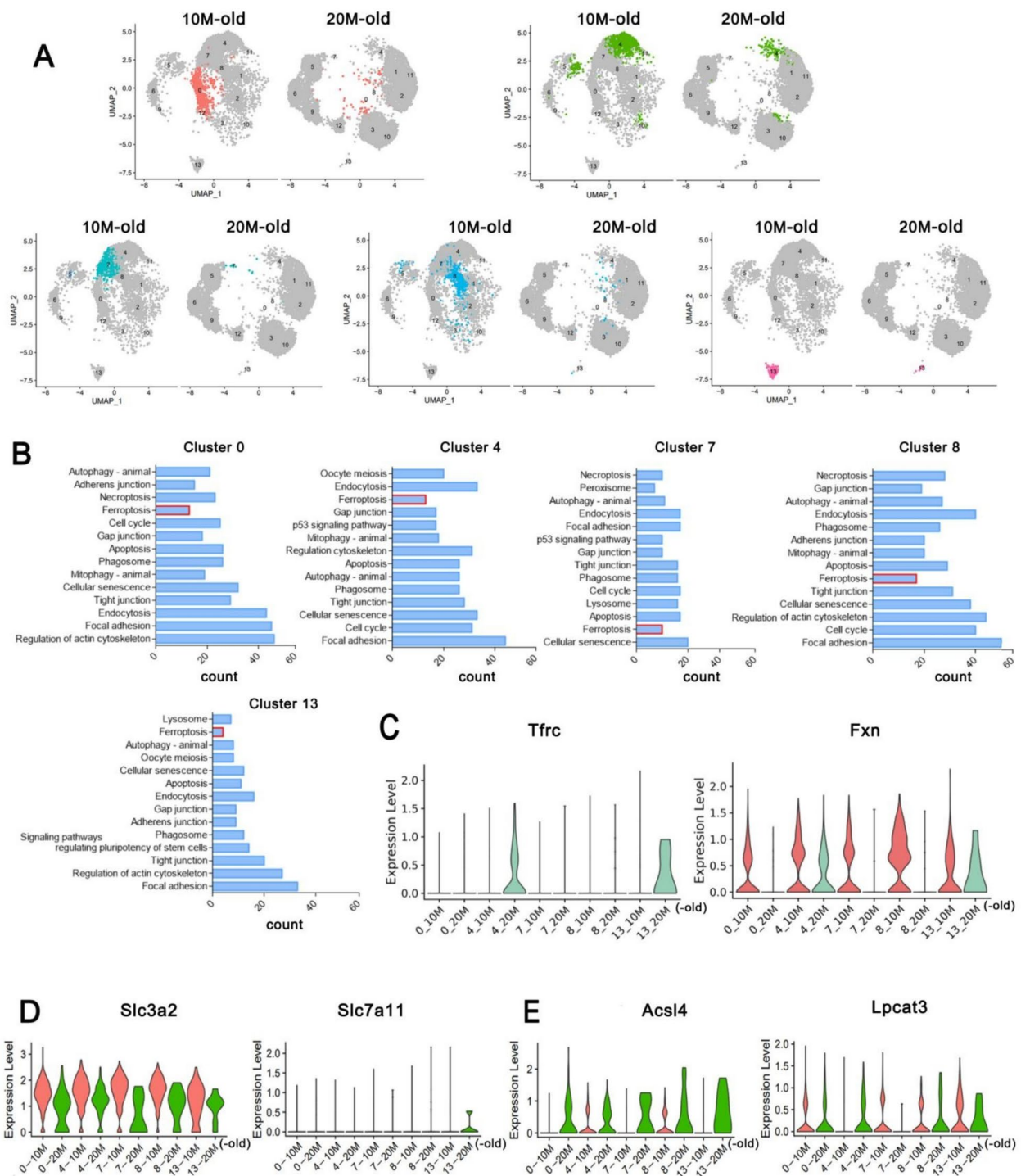


**Fig. 5** Ferroptosis-related genes and pathways are dysregulated in NP cells during IDD. **A** UMAP plots of NP cells subpopulations 0,4,7,8, and 13 (named subgroup-a) in 10 and 20M-old rat IVDs. **B** GO enrichment analysis of highly expressed genes in Group-a cells in the rat degenerative IVDs, and the top 14 biological process are shown. **C** Violin plot shows the expression levels of Tfr3 and Fxn in 10 and 20M-old rat NP cells of subgroup-a. **D** Violin plot shows the expression levels of Slc3a2 and Slc7a11 in 10 and 20M-old rat NP cells of subgroup-a. **E** Violin plot shows the expression levels of Acs14 and Lpcat3 in 10 and 20M-old rat NP cells of subgroup-a

concentration (Fig. 5C). Besides, the expression of system Xc- functional gene Slc3a2 in the 20M-old group was down-regulated, and Slc7a11 was only expressed in a small number of NP cells, which suggests an impaired glutathione reduction in NP cells (Fig. 5D). Furthermore, Acsl4 and Lpcat3, the key factors for regulating cell membrane lipid peroxidation to induce ferroptosis, were also dysregulated in the 5 clusters (Fig. 5E). Particularly, Acsl4 was significantly up-regulated in the 5 NP cell clusters, indicating an enhanced irreversible damage of cell membranes due to lipid peroxidation (Fig. 5E). Taken together, these results demonstrated that ferroptosis occurs in several NP cell populations during IDD, which contributes to the reduction of functional NP cells and to ultimately promoting the progression of IDD.

### Atf3 is a crucial driver of NP cell ferroptosis

To elucidate the factors driving the ferroptosis of NP cell subpopulations during IDD, we analyzed the expression of the 15 ferroptosis related driver genes shown in Table 1 in NP cell subpopulations. The results showed that Scp2 was up-regulated only in cluster 6, while no significant changes were observed in other NP cell clusters (Fig. 6A). Compared with the 10M-old group, the expression of Tf, Atf3, Nr1d1 and Kdm5c in the ferroptotic NP cells of 20M-old group was more up-regulated (Fig. 6A). To further identify the key factors regulating the 5 ferroptotic NP cell subsets, we found that Atf3 was most dramatically up-regulated in the notochordal cell subpopulation according to ScRNA-seq (Fig. 6B-C). In addition, Atf3, Epas1, and Nr1 d1 were more up-regulated in ferroptotic NP cell clusters 0, 4, 7, and 8 (Fig. 6D-E). Notably, compared with the 10M-old, Atf3 was the TOP2 up-regulated gene in these 5 NP cell subpopulations (Fig. 6D-E). Consistently, recent studies have found that Atf3 is up-regulated in IDD and promotes NP cells ferroptosis to mediate TBHP-induced IDD [44, 45]. Herein, we further demonstrated the upregulation of Atf3 on the single-cell UMAP of rat NP tissues in the 20M-old group (Fig. 6F). Immunofluorescence staining of NP tissues also showed an augmented signal intensity of Atf3 (Fig. 6G). Furthermore, ferroptosis of NP cells was induced by

erastin in vitro (sFigure 1 A-B). The expression of Atf3 was also significantly up-regulated by erastin treatment, which is consistent with Acsl4 (Fig. 6H-I). These results suggest that Atf3 is a typical and key ferroptosis driver of NP cells.

### Rps6 +/Cxcl1 – is a molecular feature of ferroptotic NP cells

Gene targeted therapy is one of the key treatment strategies for multiple clinical diseases, including IDD [46–50]. To identify common characteristic genes of ferroptotic NP cells, we used ScRNA-seq data to compare the average gene expression of NP cells from clusters 0, 4, 7, 8, and 13 (named subgroup-a) with that from clusters 1, 2, 3, 5, 6, 9, 10, 11 and 12 (named subgroup-b) (Fig. 7A). The gene set with high expression in subgroup-a was obtained by overlapping the TOP300 differentially expressed genes between the two subgroups with the genes with the specificity  $(a/b) > 10$  (Fig. 7B). Furthermore, a similar overlapping method  $(b-a, b/a > 10)$  was used to obtain the gene set with low expression in subgroup-a (Fig. 7B). Analysis results showed that among the 11 genes obtained, 7 were highly expressed and 4 were low expressed. Moreover, the expression of these 11 genes in each NP cell subpopulation was analyzed based on the gene expression heat map of ScRNA-seq. Rps6 was identified as a specifically high expression marker gene of the subgroup-a, while Cxcl1 was identified as a specifically low expression gene of the subgroup-a (Fig. 7C). Consistently, the violin plot also showed that Rps6 and Cxcl1 were able to distinguish the two NP cell subgroups with ideal expression specificity (Fig. 7D). Also, Rps6 + and Cxcl1 – can accurately label the ferroptotic NP cell cluster in the UMAP map (Fig. 7E). In summary, Rps6 +/Cxcl1 – is a promising molecular marker of ferroptotic NP cells during IDD.

To demonstrate that Rps6 +/Cxcl1- is a molecular marker of ferroptotic NP cells, erastin was used to induce ferroptosis of rat NP cells. The results showed that compared with the control group, the viability of NP cells was significantly inhibited by erastin (sFigure 1 A). Flow cytometry showed that the lipid peroxidation level of NP cells treated by erastin was significantly increased

(See figure on next page.)

**Fig. 6** Atf3 expression is up-regulated in ferroptosis NP cells subsets of rat IVDs. **A** Heat map shows the expression levels of 15 ferroptosis-related genes in NP cell subsets of 10 and 20M-old rats. **B** The expression of ferroptosis-related genes in notochord NP cells of 10 and 20M-old rat IVDs. **C** The proportion changes (up-regulated) of ferroptosis-related genes in notochord NP cells during IDD. **D** The expression of ferroptosis-related genes in chondrocyte-like NP cell subsets 0, 4, 7 and 8 of 10 and 20M-old rat IVDs. **E** The proportion changes (up-regulated) of ferroptosis-related genes in chondrocyte-like NP cell subsets 0, 4, 7 and 8 during IDD. **F** UMAP plot of Atf3 expression in NP cells from 10 and 20M-old rats. **G** Immunofluorescence staining of 10 and 20M-old rat tail IVD sections, with magnified representative images of NP tissue cells at right. Scale bars, 50  $\mu$ m.  $n = 3$ . **H-I** The primary NP cells cultured in the three groups were incubated with PBS, DMSO or DMSO + Erastin for 24 h, respectively, and then the cells were collected. The mRNA expression levels of Atf3 (**H**) and Acsl4 (**I**) were detected by Real-Time PCR. Data are expressed as the mean  $\pm$  SEM ( $n = 3$ ). \* $P < 0.05$ , \*\* $P < 0.01$ , NS, no significance

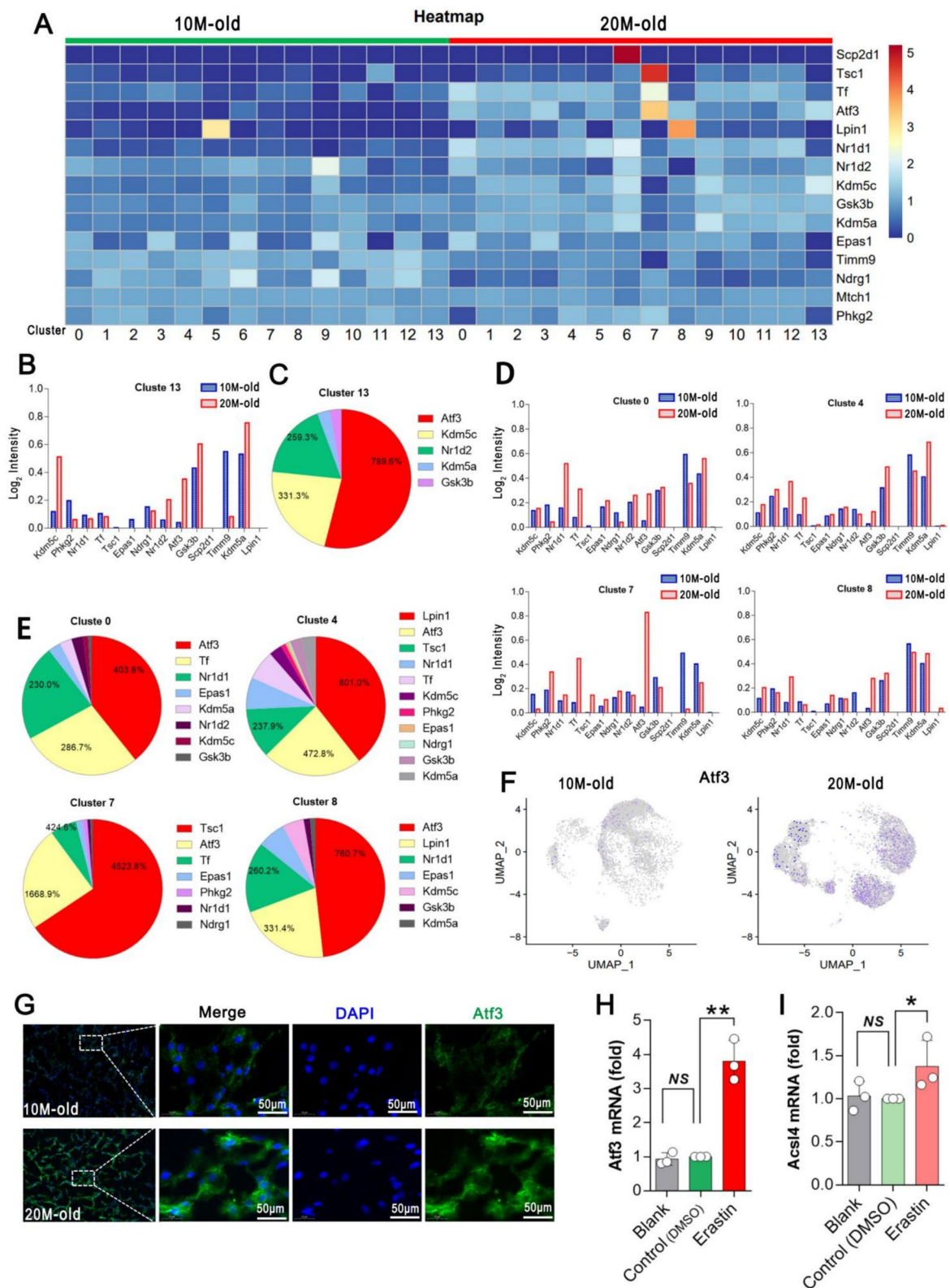


**Fig. 6** (See legend on previous page.)

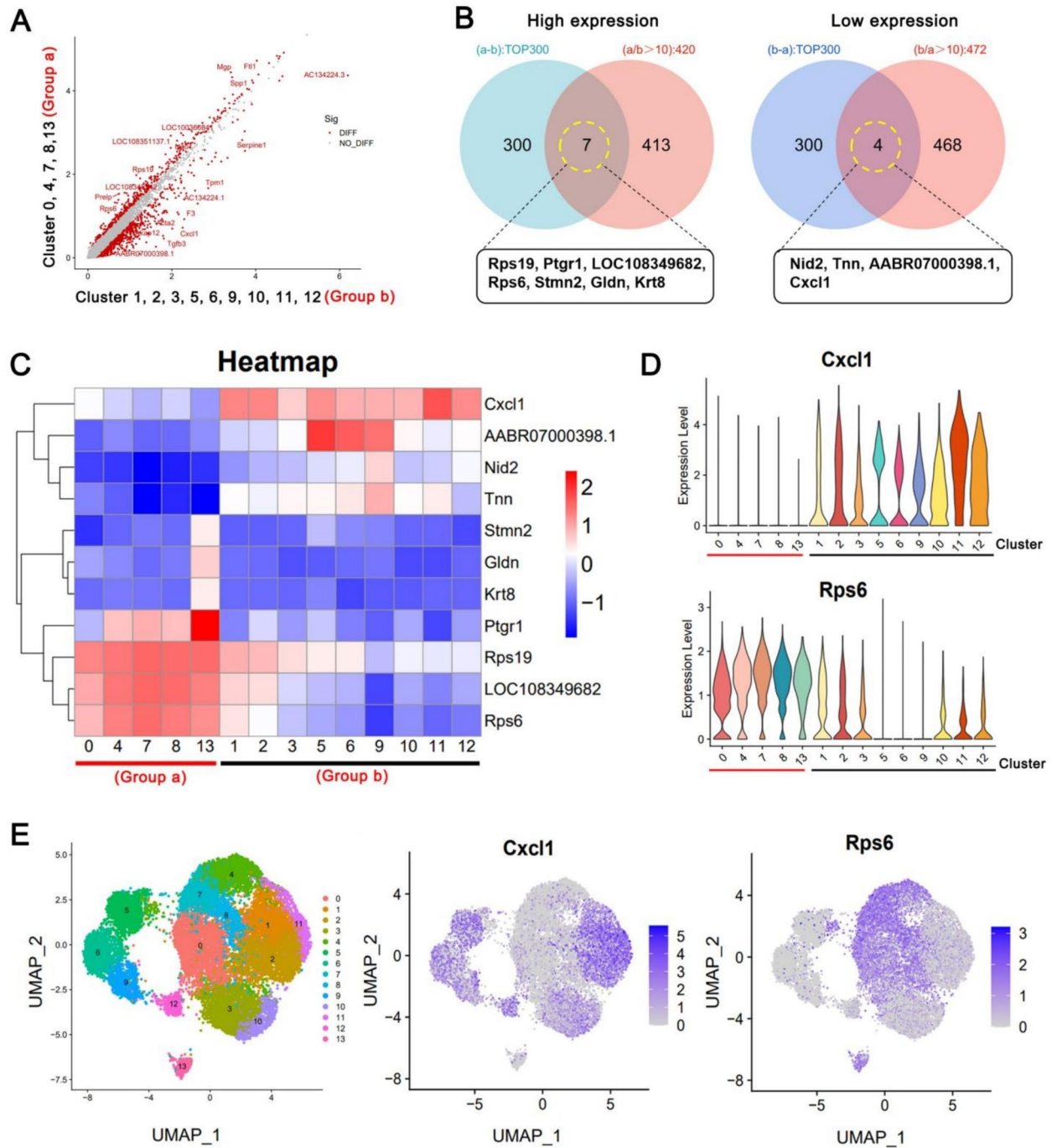


**Fig. 7** Cross enrichment analysis identifies the common maker of 5 ferroptotic NP cell clusters. **A** Scatter plot reveals the differences of genes average expression levels in rat NP cell clusters 0, 4, 7, 8 and 13 (named subgroup-a) and 1, 2, 3, 5, 6, 9, 10, 11, 12 (named subgroup-b). **B** The top 300 in (a-b) with (a/b) > 10 genes were cross-enriched to obtain the genes highly expressed in subgroup-a (left). In addition, the top 300 in (b-a) with (b/a) > 10 genes were cross-enriched to obtain the genes that are low expressed in subgroup-a (right). **C** Heat map shows the average expression levels of the genes obtained by enrichment analysis in the cell subsets of subgroup-a and subgroup-b. **D** Violin plot shows the expression levels of Cxcl1 and Rps6 in rat IVD NP cell subsets of group-a and subgroup-b. **E** UMAP plots of Cxcl1 and Rps6 expression distribution in NP cell subsets

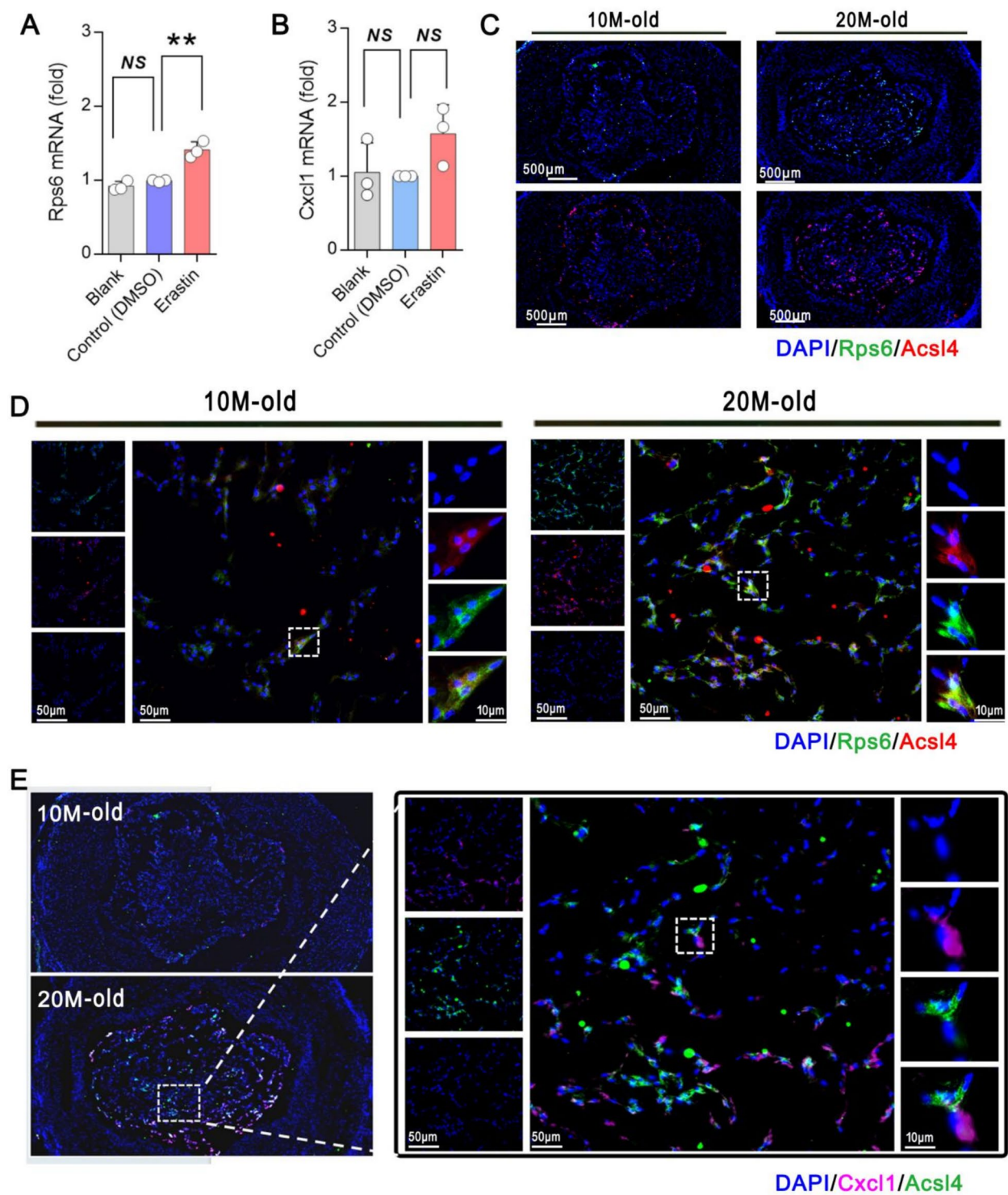


**Fig. 8** Validation of maker genes associated with ferroptotic NP cell subsets. **A-B** The primary NP cells cultured in the three groups were incubated with PBS, DMSO or DMSO + Erastin for 24 h, respectively, and then the cells were collected. The mRNA expression levels of Rps6 (**A**) and Cxcl1 (**B**) were detected by Real-Time PCR. Data are expressed as the mean  $\pm$  SEM ( $n = 3$ ). **(C-D)** Immunofluorescence staining (Rps6 and Acs14) of 10 and 20M-old rat tail IVD cross sections. Scale bars, 500  $\mu$ m (**C**), Scale bars, 50 or 10  $\mu$ m (**D**). **E** Immunofluorescence staining (Cxcl1 and Acs14) of 10 and 20M-old rat tail IVD cross sections. Representative images of enlarged NP cells are shown on the right. Scale bars, 50 or 10  $\mu$ m. **\*\*** $P < 0.01$ , **NS**, no significance

(sFigure 1B). In addition, Real-time PCR results further showed that the transcription of *Rps6* was significantly up-regulated (Fig. 8A). However, there was no significant difference in *Cxcl1* transcription (Fig. 8B). Moreover, the immunofluorescence staining of *Rps6* and *Cxcl1* was performed on 10 and 20M-old rat IVDs. Results showed that, compared with the 10M-old, the NP cells with high expression of *Rps6* increased in the 20M-old group, and the fluorescence intensity of *Acl4* was also consistently up-regulated in the NP cells with high expression of *Rps6* (Fig. 8C). Importantly, NP cells showed colocalized expression of *Rps6* and *Acl4* (Fig. 8D). On the other hand, *Cxcl1* expression is increased in degenerative rat NP tissues, but there was little overlap between *Cxcl1* expression and *Acl4* expression in NP cells (Fig. 8E). These results indicate that *Rps6* +/*Cxcl1*- is a molecular feature of ferroptotic NP cells.

## Discussion

In this study, we found the accumulation of iron in rat NP tissues with aging. Also, an enhanced lipid peroxidation and increased lipid peroxidation products were shown in aging NP tissues. It suggests NP cell ferroptosis with the development of IDD. Furthermore, with the conjoint analysis of ScRNA-seq of NP cells and Bulk RNA-seq analysis of NP tissues, ATF3 was identified as a key factor driving NP cell ferroptosis. On the other hand, we further demonstrated that *Rps6* +/*Cxcl1*- is a common molecular feature of ferroptotic NP cell subpopulations, which provides a new insight into targeting the delay or treatment of IDD.

There is growing evidence that multiple types of cell death lead to the reduction of functional NP cells which is associated with the progression of IDD [51–53]. Ferroptosis is a new type of programmed cell death, and its mechanism and characteristics in IDD have not been clearly elucidated [23, 54]. Recently, ferroptosis-related genes and signaling pathways were found to be enriched in NP cells of human and rat degenerative IVDs, indicating an important role of NP cell ferroptosis in IDD [54, 55]. Herein, we also found an enhanced ferroptosis of NP cells in rat degenerative IVDs. 15 ferroptosis-related genes of NP cells were identified by the overlapping analysis of Bulk RNA-seq of rat NP tissues and FerrDb database. GO and KEGG analysis showed that these genes were mainly enriched in cell proliferation and apoptosis, lipid metabolism, mitochondrial and outer membrane composition, ferroptosis, etc., suggesting an association of NP cell ferroptosis with the pathogenesis of IDD. Therefore, it is of great importance to further investigate the key ferroptosis driving genes and the characteristics of ferroptotic NP cells in degenerated IVDs.

Based on the clustering analysis of ScRNA-seq, we divided rat IVD NP cells into two main categories: notochordal NP cells and chondrocyte-like NP cells. Mature chondrocyte-like NP cells are further divided into 13 subsets according to their different transcriptome profiles, which play their respective regulatory functions in NP tissues (such as matrix formation, cartilage development, stress tolerance, etc.). In addition, notochordal NP cells, as the precursors of mature NP cells, play an extremely important role in the regeneration and differentiation of mature chondrocyte-like NP cells [56, 57]. In recent years, researchers have extensively explored notochordal NP cells in human and bovine, and identified *Krt8* and *Stmn2* as the marker genes [36, 37, 56]. Herein, *Krt7* is a new marker molecule of notochordal NP cells that we have found in rat IVDs. More and more studies have shown that notochordal NP cells with progenitor cell characteristics gradually disappear during IDD, and the inducible factors remain unclear [57, 58]. Importantly, for the first time, we found that the imbalance of iron metabolism and increased lipid peroxidation in notochordal NP cells caused cell ferroptosis, and further reduced its number, which provided additional evidence for the disappearance of notochordal NP cells in IDD progression.

Atf3 is a highly conserved transcription factor with molecular weight of 21kDa. It acts as a transcriptional repressor or activator by interacting with ATF/CREB family members or binding to the promoters of target genes [59, 60]. During IDD, the expression of *Atf3* in NP cells is abnormally increased, and its silencing can delay the process of IDD by inhibiting ferroptosis, apoptosis and ECM degradation of NP cells [45]. Moreover, *Atf3* promoted the recruitment of macrophages to participate in IDD progression by activating CCL2/7-CCR2 signaling pathway in NP cells [61]. These studies suggest that *Atf3* plays a crucial role in the occurrence and development of IDD. More importantly, recent studies have reported that *Atf3* is one of the hub genes inducing ferroptosis in various diseases including cancer, liver fibrosis and acute lung injury [62–64]. In the current study, we found that the expressions of *Tsc1*, *Tf*, *Atf3*, *Lpin1*, etc. were significantly up-regulated in ferroptotic NP cell subpopulations. Notably, *Atf3* is the only gene within the TOP2 up-regulated genes of the 5 ferroptotic NP cell subpopulations and is shown to be significantly up-regulated in rat aging-related IDD and erastin treated NP cells, indicating its unique and critical role in NP cell ferroptosis. However, *Atf3* was partially up-regulated in other NP cell subpopulations and may play different biological functions. The targeted regulation of *Atf3* expression in ferroptotic NP cell subpopulations is a promising strategy for delaying and treating IDD.

Rps6, also known as phosphoprotein NP33, is a ribosomal protein belonging to the 40S small ribosomal subunit [65, 66]. Rps6 is considered as a stimulator or inhibitor of certain protein synthesis and plays an important regulatory role in cell metabolic balance, aging, proliferation and apoptosis [67–70]. In fact, unphosphorylated Rps6 and phosphorylated Rps6 (p-Rps6) have different functions in regulating cell fate. For example, unphosphorylated Rps6 in tumor cells is a selective mediator of TRAIL-induced apoptosis [71]. It has been reported that unphosphorylated Rps6 is not only the inactive form of p-Rps6, but its N terminus also has pro-apoptotic activity, which can sensitize HeLa cells to TRAIL. Unphosphorylated Rps6 is a specific highly expressed molecule for cell death [57]. On the other hand, p-Rps6 has been shown to be strongly associated with cell senescence and death. Alessio et al. reported that Ki67 (–), p-Rps6 (+) and SA-β-gal (+) are typical markers of senescent cells [72]. Furthermore, in oocytes, decreased WIP1 expression accelerates aging throughout the ovary by activating Rps6 phosphorylation to promote primal follicle depletion [73]. These studies suggest that different modified forms of Rps6 play an important role in cell senescence and death. In our study, we found that Rps6 was highly expressed specifically in ferroptotic NP cells. More importantly, Rps6 was co-expressed with *Acs14* in NP tissues, suggesting that Rps6 is a potential biomarker of NP cell ferroptosis. However, it is necessary to point out that the correlation between Rps6 and *Atf3* in NP cells and the exact roles of Rps6 in NP cell ferroptosis are still unclear. Furthermore, as the effects of phosphorylation or unphosphorylation of Rps6 on NP cell ferroptosis and IDD remain to be further elucidated.

*Cxcl1* gene is located at the 4q12-q13 CXC chemokine gene cluster [74]. In 1987, *Cxcl1* has been shown to be a product of the growth regulatory gene [75]. *Cxcl1* is also one of the most important chemokines and is mainly involved in the development of many inflammatory diseases. Especially in aging-related diseases, the up-regulation of chemokine *Cxcl1* induces the migration and infiltration of neutrophils, thus promoting the development of inflammation [76]. Besides, *Cxcl1* promotes the proliferation of tumor cells [77, 78]. *Cxcl1* is a potential biomarker of reactive activation and proliferation of cells, mediating the clearance of damaged and dead cells, as well as tissue repair. It is one of the most significantly up-regulated inflammatory cytokines in aging dermal white adipose tissues [79]. In the inflammatory phase of wound healing, *Cxcl1* causes the recruitment of neutrophils, which leads to the clearance of pathogens and diseased cells from the damaged skin [80]. Moreover, treatment of primary mesenchymal stromal cells isolated from human osteoarthritis cartilage with recombinant Shh

significantly increased cell number and proliferation rate, activated the expression of chondrogenic markers *Col2a1* and *Acan*, and *Cxcl1* [81]. Consistent with the previous studies, *Cxcl1* was mainly expressed in some aging and inflammatory NP cell subsets of degenerative rat IVDs, which may be a senescence-associated secretory phenotype (SASP) that accompanies degenerative diseases. On the other hand, *Cxcl1* was not expressed in ferroptotic NP cells. Thus, it is a promising biomarker to distinguish NP cell ferroptosis.

However, there are some limitations in our study. We used NP tissues and NP cells from male rat caudal IVDs for mRNA-seq and ScRNA-seq, ignoring possible bias due to the gender. In addition, due to the biomechanical environment, circadian rhythm and aging process of rat tail IVDs are different from that of human IVDs. Moreover, we only focused on rats aging related degeneration, and the other degeneration causes were not considered. Further studies on the characteristics of ferroptosis NP cells in different animal models and human samples (male and female) will provide a perspective to fully understand the relationship between ferroptosis and aging-related IDD. Besides, according to our previous results, the three age groups of rats have different degeneration characteristics, the time and gene regulatory mechanisms of cell death may be also different. Therefore, in the future studies, comprehensive analysis of the ferroptosis related gene changes in IVDs at different ages will further explain the key role of NP cell ferroptosis in aging-related IDD, which might provide an important preliminary theoretical basis for the subsequent study of clinical diagnosis and targeted gene therapy in IDD.

## Conclusion

In conclusion, our study demonstrates that NP cell ferroptosis is associated with the development of IDD. *Atf3* is a key factor inducing ferroptosis of NP cells. Moreover, Rps6 +/*Cxcl1* – is a promising common molecular feature of ferroptotic NP cell subpopulations. These findings provide important clues for further elucidating the mechanism of NP cell ferroptosis and exploring gene-targeted therapeutic strategies for IDD.

## Abbreviations

IDD	Intervertebral disc degeneration
NP	Nucleus pulposus
IVD	Intervertebral disc
10M-old	10 months old
20M-old	20 months old
4-HNE	4-Hydroxynonenal
C11-BODIPY	Undecanoyl Boron Dipyrromethene
<i>Acs14</i>	Acyl-CoA synthase long chain family member 4
<i>Lpcat3</i>	Lysophosphatidylcholine acyltransferase 3
PUFA	Polyunsaturated fatty acids
PL	Phospholipids
SD	Sprague–Dawley
PFA	Paraformaldehyde

ScRNA-seq	Single cell sequencing
Bulk RNA-seq	RNA sequencing of bulk samples
DEGs	Differentially expressed genes
CCK-8	Cell Counting Kit-8
OAF	Outer annulus fibrosus
IAF	Internal annulus fibrosus
KEGG	Kyoto Encyclopedia of Genes and Genomes
GO	Gene Ontology
Tfrc/Tfr1	Transferrin receptor protein 1
Fxn	Frataxin
p-Rps6	Phosphorylated Rps6
SASP	Senescence-associated secretory phenotype

## Supplementary Information

The online version contains supplementary material available at <https://doi.org/10.1186/s13075-025-03550-7>.

Supplementary Material 1

## Acknowledgements

Not applicable.

## Authors' contributions

SP Chen performed the experiments, analyzed the data, and wrote this paper; JW Fu and J Long analyzed the data and wrote this paper; C Liu, XZ Ai and D Long performed the experiments and analyzed the data; X Leng, Y Zhang and ZG Liao edited the manuscript; CQ Li, and Y Zhou designed the paper; SW Dong, B Huang and CC Feng conceived, designed and wrote the paper. All authors reviewed and approved the final manuscript.

## Funding

This study was supported by National Natural Science Foundation of China (82372467, 81972114, 82072495), Natural Science Foundation of Chongqing in China (CSTB2024 NSCQ-MSX1155).

## Data availability

The data that support the findings of this study are available from the online supplemental materials or from the corresponding author upon reasonable request. RNA-seq raw data reported in this paper have been deposited in the Gene Expression Omnibus (GEO) database (<https://www.ncbi.nlm.nih.gov/GSE234369>).

## Declarations

### Ethics approval and consent to participate

Male SD rats were obtained from the Animal Center of Second Affiliated Hospital, Army Medical University, Chongqing, China. All experimental procedures were approved by the hospital Animal Ethics Committee (Registration approval number: AMUWEC2020088).

### Consent for publication

Not applicable.

### Competing interests

The authors declare no competing interests.

### Author details

<sup>1</sup>Department of Orthopedics, Xinqiao Hospital, Army Medical University, Chongqing 400037, P. R. China. <sup>2</sup>Chongqing Municipal Health Commission Key Laboratory of Precise Orthopedics, Chongqing, China. <sup>3</sup>Department of Biomedical Materials Science, School of Biomedical Engineering, Army Medical University, Chongqing, China. <sup>4</sup>State Key Laboratory of Trauma, Burns and Combined Injury, Army Medical University, Chongqing, China.

Received: 21 October 2024 Accepted: 27 March 2025

Published online: 17 April 2025

## References

- Chou R. Low Back Pain (2021). *Ann Intern Med*, 174(8):ITC113-ITC128.
- Maier C, Underwood M, Buchbinder R. Non-specific low back pain (2017). *Lancet*, 389(10070):736–747.
- Vos T, Flaxman AD, Naghavi M, Lozano R, Michaud C, Ezzati M, et al. Years lived with disability (YLDs) for 1160 sequelae of 289 diseases and injuries 1990–2010: a systematic analysis for the Global Burden of Disease Study 2010. *Lancet*. 2012;380(9859):2163–96.
- Feng C, Liu H, Yang M, Zhang Y, Huang B, Zhou Y. Disc cell senescence in intervertebral disc degeneration: Causes and molecular pathways. *Cell Cycle*. 2016;15(13):1674–84.
- Vo N, Niedernhofer LJ, Nasto LA, Jacobs L, Robbins PD, Kang J, et al. An overview of underlying causes and animal models for the study of age-related degenerative disorders of the spine and synovial joints. *J Orthop Res*. 2013;31(6):831–7.
- Wang Y, Wang H, Zhuo Y, Hu Y, Zhang Z, Ye J, et al. SIRT1 alleviates high-magnitude compression-induced senescence in nucleus pulposus cells via PINK1-dependent mitophagy. *Aging (Albany NY)*. 2020;12(16):16126–41.
- Yin X, Motorwala A, Vesvoranan O, Levene HB, Gu W, Huang CY. Effects of Glucose Deprivation on ATP and Proteoglycan Production of Intervertebral Disc Cells under Hypoxia. *Sci Rep*. 2020;10(1):8899.
- Wang Y, Che M, Xin J, Zheng Z, Li J, Zhang S. The role of IL-1 $\beta$  and TNF- $\alpha$  in intervertebral disc degeneration. *Biomed Pharmacother*. 2020;131:110660.
- Chen Z, Chen C, Yang X, Zhou Y, Cao X, Han C, et al. Dysfunction of STING Autophagy Degradation in Senescent Nucleus Pulposus Cells Accelerates Intervertebral Disc Degeneration. *Int J Biol Sci*. 2024;20(7):2370–87.
- Peng P, Wang D, Xu X, Wang D, Gao B, Wang H, et al. Targeting clock-controlled gene Nrf2 ameliorates inflammation-induced intervertebral disc degeneration. *Arthritis Res Ther*. 2022;24(1):181.
- Xu J, Shao T, Lou J, Zhang J, Xia C. Aging, cell senescence, the pathogenesis and targeted therapies of intervertebral disc degeneration. *Front Pharmacol*. 2023;14:1172920.
- Wang F, Cai F, Shi R, Wang XH, Wu XT. Aging and age related stresses: a senescence mechanism of intervertebral disc degeneration. *Osteoarthritis and cartilage / OARS, Osteoarthritis Research Society*. 2016;24(3):398–408.
- Jia C, Xiang Z, Zhang P, Liu L, Zhu X, Yu R, et al. Selenium-SelK-GPX4 axis protects nucleus pulposus cells against mechanical overloading-induced ferroptosis and attenuates senescence of intervertebral disc. *Cell Mol Life Sci*. 2024;81(1):49.
- Yurube T, Takeoka Y, Kanda Y, Kuroda R, Kakutani K. Intervertebral disc cell fate during aging and degeneration: apoptosis, senescence, and autophagy. *N Am Spine Soc J*. 2023;14:100210.
- Dixon SJ, Lemberg KM, Lamprecht MR, Skouta R, Zaitsev EM, Gleason CE, et al. Ferroptosis: an iron-dependent form of nonapoptotic cell death. *Cell*. 2012;149(5):1060–72.
- Tang D, Kroemer G. Ferroptosis (2020). *Curr Biol*, 30(21):R1292-R1297.
- Liu J, Kang R, Tang D. Signaling pathways and defense mechanisms of ferroptosis. *FEBS J*. 2022;289(22):7038–50.
- Cui J, Wang Y, Tian X, Miao Y, Ma L, Zhang C, et al. LPCAT3 Is Transcriptionally Regulated by YAP/ZEB/EP300 and Collaborates with ACSL4 and YAP to Determine Ferroptosis Sensitivity. *Antioxid Redox Signal*. 2023;39(7–9):491–511.
- Oda K, Lee Y, Wiriyasermkul P, Tanaka Y, Takemoto M, Yamashita K, et al. Consensus mutagenesis approach improves the thermal stability of system Xc- transporter, xCT, and enables cryo-EM analyses. *Protein Sci*. 2020;29(12):2398–407.
- Lin W, Wang C, Liu G, Bi C, Wang X, Zhou Q, et al. SLC7A11/xCT in cancer: biological functions and therapeutic implications. *Am J Cancer Res*. 2020;10(10):3106–26.
- Hong T, Lei G, Chen X, Li H, Zhang X, Wu N, et al. PARP inhibition promotes ferroptosis via repressing SLC7A11 and synergizes with ferroptosis inducers in BRCA-proficient ovarian cancer. *Redox Biol*. 2021;42:101928.
- Xiang P, Chen Q, Chen L, Lei J, Yuan Z, Hu H, et al. Metabolite Neu5Ac triggers SLC3A2 degradation promoting vascular endothelial ferroptosis and aggravates atherosclerosis progression in ApoE-/- mice. *Theranostics*. 2023;13(14):4993–5016.

23. Xiang Q, Zhao Y, Li W. Identification and validation of ferroptosis-related gene signature in intervertebral disc degeneration. *Front Endocrinol (Lausanne)*. 2023;14:1089796.
24. Fernandes LM, Khan NM, Trochez CM, Duan M, Diaz-Hernandez ME, Presciutti SM, et al. Single-cell RNA-seq identifies unique transcriptional landscapes of human nucleus pulposus and annulus fibrosus cells. *Sci Rep*. 2020;10(1):15263.
25. Li Z, Ye D, Dai L, Xu Y, Wu H, Luo W, et al. Single-Cell RNA Sequencing Reveals the Difference in Human Normal and Degenerative Nucleus Pulposus Tissue Profiles and Cellular Interactions. *Front Cell Dev Biol*. 2022;10: 910626.
26. Feng C, Yang M, Lan M, Liu C, Zhang Y, Huang B, et al. ROS: Crucial Intermediators in the Pathogenesis of Intervertebral Disc Degeneration. *Oxid Med Cell Longev*. 2017;2017:5601593.
27. Zhuang Y, Liu L, Liu M, Fu J, Ai X, Long D, et al. The sonic hedgehog pathway suppresses oxidative stress and senescence in nucleus pulposus cells to alleviate intervertebral disc degeneration via GPX4. *Biochim Biophys Acta Mol Basis Dis*. 2024;1870(2): 166961.
28. Liu L, Zhang Y, Fu J, Ai X, Long D, Leng X, et al. Gli1 depletion induces oxidative stress and apoptosis of nucleus pulposus cells via Fos in intervertebral disc degeneration. *J Orthop Translat*. 2023;40:116–31.
29. Liu L, Sun H, Zhang Y, Liu C, Zhuang Y, Liu M, et al. Dynamics of N6-methyladenosine modification during aging and their potential roles in the degeneration of intervertebral disc. *JOR Spine*. 2024;7(1): e1316.
30. Wang Y, Zhao J, Chen S, Li D, Yang J, Zhao X, et al. Let-7 as a Promising Target in Aging and Aging-Related Diseases: A Promise or a Pledge. *Biomolecules*. 2022;12(8):1070.
31. Tong T, Liu Z, Zhang H, Sun J, Zhang D, Wang F, et al. Age-dependent expression of the vitamin D receptor and the protective effect of vitamin D receptor activation on H2O2-induced apoptosis in rat intervertebral disc cells. *J Steroid Biochem Mol Biol*. 2019;190:126–38.
32. Chen HW, Liu MQ, Zhang GZ, Zhang CY, Wang ZH, Lin AX, et al. Proanthocyanidins inhibit the apoptosis and aging of nucleus pulposus cells through the PI3K/Akt pathway delaying intervertebral disc degeneration. *Connect Tissue Res*. 2022;63(6):650–62.
33. Kamatani T, Hagizawa H, Yarimitsu S, Morioka M, Koyamatsu S, Sugimoto M, et al. Human iPS cell-derived cartilaginous tissue spatially and functionally replaces nucleus pulposus. *Biomaterials*. 2022;284: 121491.
34. McCann MR, Tamplin OJ, Rossant J, Séguin CA. Tracing notochord-derived cells using a Noto-cre mouse: implications for intervertebral disc development. *Dis Model Mech*. 2012;5(1):73–82.
35. Xia K, Gong Z, Zhu J, Yu W, Wang Y, Wang J, et al. Differentiation of Pluripotent Stem Cells into Nucleus Pulposus Progenitor Cells for Intervertebral Disc Regeneration. *Curr Stem Cell Res Ther*. 2019;14(1):57–64.
36. Rodrigues-Pinto R, Ward L, Humphreys M, Zeef LAH, Berry A, Hanley KP, et al. Human notochordal cell transcriptome unveils potential regulators of cell function in the developing intervertebral disc. *Sci Rep*. 2018;8(1):12866.
37. Rodrigues-Pinto R, Berry A, Piper-Hanley K, Hanley N, Richardson SM, Hoyland JA. Spatiotemporal analysis of putative notochordal cell markers reveals CD24 and keratins 8, 18, and 19 as notochord-specific markers during early human intervertebral disc development. *J Orthop Res*. 2016;34(8):1327–40.
38. Tu J, Li W, Yang S, Yang P, Yan Q, Wang S, et al. Single-Cell Transcriptome Profiling Reveals Multicellular Ecosystem of Nucleus Pulposus during Degeneration Progression. *Adv Sci (Weinh)*. 2022;9(3): e2103631.
39. Han S, Zhang Y, Zhang X, Zhang H, Meng S, Kong M, et al. Single-Cell RNA Sequencing of the Nucleus Pulposus Reveals Chondrocyte Differentiation and Regulation in Intervertebral Disc Degeneration. *Front Cell Dev Biol*. 2022;10: 824771.
40. Rochette L, Dogon G, Rigal E, Zeller M, Cottin Y, Vergely C. Lipid Peroxidation and Iron Metabolism: Two Corner Stones in the Homeostasis Control of Ferroptosis. *Int J Mol Sci*. 2022;24(1):449.
41. Song X, Zhu S, Chen P, Hou W, Wen Q, Liu J, et al. AMPK-Mediated BECN1 Phosphorylation Promotes Ferroptosis by Directly Blocking System Xc-Activity. *Curr Biol*. 2018;28(15):2388–2399.e5.
42. Zhou X, Fu Y, Liu W, Mu Y, Zhang H, Chen J, et al. Ferroptosis in Chronic Liver Diseases: Opportunities and Challenges. *Front Mol Biosci*. 2022;9: 928321.
43. Du J, Zhou Y, Li Y, Xia J, Chen Y, Chen S, et al. Identification of Frataxin as a regulator of ferroptosis. *Redox Biol*. 2020;32: 101483.
44. Guo J, Yang Y, Niu J, Luo Z, Shi Q, Yang H. Establishment of Ferroptosis-Related Key Gene Signature and Its Validation in Compression-Induced Intervertebral Disc Degeneration Rats. *Oxid Med Cell Longev*. 2023;2023:9020236.
45. Li Y, Pan D, Wang X, Huo Z, Wu X, Li J, et al. Silencing ATF3 Might Delay TBHP-Induced Intervertebral Disc Degeneration by Repressing NPC Ferroptosis, Apoptosis, and ECM Degradation. *Oxid Med Cell Longev*. 2022;2022:4235126.
46. Zhang XB, Hu YC, Cheng P, Zhou HY, Chen XY, Wu D, et al. Targeted therapy for intervertebral disc degeneration: inhibiting apoptosis is a promising treatment strategy. *Int J Med Sci*. 2021;18(13):2799–813.
47. Mei L, Zheng Y, Gao X, Ma T, Xia B, Hao Y, et al. Hsa-let-7f-1-3p targeting the circadian gene Bmal1 mediates intervertebral disc degeneration by regulating autophagy. *Pharmacol Res*. 2022;186: 106537.
48. Chen S, Guan L, Zhao X, Yang J, Chen L, Guo M, et al. Optimized thyroid transcription factor-1 core promoter-driven microRNA-7 expression effectively inhibits the growth of human non-small-cell lung cancer cells. *J Zhejiang Univ Sci B*. 2022;23(11):915–30.
49. Chen S, Wang Y, Li D, Wang H, Zhao X, Yang J, et al. Mechanisms Controlling MicroRNA Expression in Tumor. *Cells*. 2022;11(18):2852.
50. Chen S, Wang H, Guo M, Zhao X, Yang J, Chen L, et al. Promoter A1312C mutation leads to microRNA-7 downregulation in human non-small cell lung cancer. *Cell Signal*. 2024;117: 111095.
51. Wu S, Liu S, Huang R, Zhou Y, Zou Y, Yang W, et al. Adiponectin inhibits LPS-induced nucleus pulposus cell pyroptosis through the miR-135a-5p/TXNIP signaling pathway. *Aging (Albany NY)*. 2023;15(23):13680–92.
52. Lin J, Zheng X, Xiong Z, Xiang Q, Zhao Y, Jiang S, et al. DJ-1-mediated p62 degradation delays intervertebral disc degeneration by inhibiting apoptosis of nucleus pulposus cells. *Apoptosis*. 2023;28(9–10):1357–71.
53. Wang Z, Li X, Yu P, Zhu Y, Dai F, Ma Z, et al. Role of Autophagy and Pyroptosis in Intervertebral Disc Degeneration. *J Inflamm Res*. 2024;17:91–100.
54. Jiang F, Li X, Xie Z, Liu L, Wu X, Wang Y. Bioinformatics Analysis and Identification of Ferroptosis-Related Hub Genes in Intervertebral Disc Degeneration. *Biochem Genet*. 2023;62(5):3403–20.
55. Li S, Liao Z, Yin H, Liu O, Hua W, Wu X, et al. G3BP1 coordinates lysophagy activity to protect against compression-induced cell ferroptosis during intervertebral disc degeneration. *Cell Prolif*. 2023;56(3): e13368.
56. Minogue BM, Richardson SM, Zeef LA, Freemont AJ, Hoyland JA. Transcriptional profiling of bovine intervertebral disc cells: implications for identification of normal and degenerate human intervertebral disc cell phenotypes. *Arthritis Res Ther*. 2010;12(1):R22.
57. Matta A, Erwin WM. Current Status of the Instructional Cues Provided by Notochordal Cells in Novel Disc Repair Strategies. *Int J Mol Sci*. 2021;23(1):427.
58. Li D, Zeng Q, Jiang Z, Ding L, Lu W, Bian M, et al. Induction of notochordal differentiation of bone marrow mesenchymal-derived stem cells via the stimulation of notochordal cell-rich nucleus pulposus tissue. *Mol Med Rep*. 2021;23(2):162.
59. Katz HR, Arcese AA, Bloom O, Morgan JR. Activating Transcription Factor 3 (ATF3) is a Highly Conserved Pro-regenerative Transcription Factor in the Vertebrate Nervous System. *Front Cell Dev Biol*. 2022;10: 824036.
60. Rodríguez-Martínez JA, Reinke AW, Bhimsaria D, Keating AE, Ansari AZ. Combinatorial bZIP dimers display complex DNA-binding specificity landscapes. *Elife*. 2017;6: e19272.
61. Tian S, Chen X, Wu W, Lin H, Qing X, Liu S, et al. Nucleus pulposus cells regulate macrophages in degenerated intervertebral discs via the integrated stress response-mediated CCL2/7-CCR2 signaling pathway. *Exp Mol Med*. 2024;56(2):408–21.
62. Lu S, Wang XZ, He C, Wang L, Liang SP, Wang CC, et al. ATF3 contributes to brucine-triggered glioma cell ferroptosis via promotion of hydrogen peroxide and iron. *Acta Pharmacol Sin*. 2021;42(10):1690–702.
63. Wang Y, Li Y, Qiu Y, Shen M, Wang L, Shao J, et al. Artesunate Induces Ferroptosis in Hepatic Stellate Cells and Alleviates Liver Fibrosis via the ROCK1/ATF3 Axis. *J Clin Transl Hepatol*. 2024;12(1):36–51.
64. Wang W, Xu R, He P, Xiong Y, Zhao H, Fu X, et al. CircEXOC5 Aggravates Sepsis-Induced Acute Lung Injury by Promoting Ferroptosis Through the IGF2BP2/ATF3 Axis. *J Infect Dis*. 2024;229(2):522–34.
65. Vladimirov SN, Ivanov AV, Karpova GG, Musolyamov AK, Egorov TA, Thiede B, et al. Characterization of the human small-ribosomal-subunit proteins by N-terminal and internal sequencing, and mass spectrometry. *Eur J Biochem*. 1996;239(1):144–9.

66. Biever A, Puighermanal E, Nishi A, David A, Panciatici C, Longueville S, et al. PKA-dependent phosphorylation of ribosomal protein S6 does not correlate with translation efficiency in striatonigral and striatopallidal medium-sized spiny neurons. *J Neurosci*. 2015;35(10):4113–30.
67. Magnuson B, Ekim B, Fingar DC. Regulation and function of ribosomal protein S6 kinase (S6K) within mTOR signalling networks. *Biochem J*. 2012;441(1):1–21.
68. Paturi S, Gutta AK, Katta A, Kakarla SK, Arvapalli RK, Gadde MK, et al. Effects of aging and gender on muscle mass and regulation of Akt-mTOR-p70s6k related signaling in the F344BN rat model. *Mech Ageing Dev*. 2010;131(3):202–9.
69. Kim JY, Burghardt RC, Wu G, Johnson GA, Spencer TE, Bazer FW. Select nutrients in the ovine uterine lumen. VIII. Arginine stimulates proliferation of ovine trophectoderm cells through MTOR-RPS6K-RPS6 signaling cascade and synthesis of nitric oxide and polyamines. *Biol Reprod*. 2011;84(1):70–8.
70. Chuang YC, Yang JL, Yang DI, Lin TK, Liou CW, Chen SD. Roles of Sestrin2 and Ribosomal Protein S6 in Transient Global Ischemia-Induced Hippocampal Neuronal Injury. *Int J Mol Sci*. 2015;16(11):26406–16.
71. Jeon YJ, Kim IK, Hong SH, Nan H, Kim HJ, Lee HJ, et al. Ribosomal protein S6 is a selective mediator of TRAIL-apoptotic signaling. *Oncogene*. 2008;27(31):4344–52.
72. Alessio N, Aprile D, Cappabianca S, Peluso G, Di Bernardo G, Galderisi U. Different Stages of Quiescence, Senescence, and Cell Stress Identified by Molecular Algorithm Based on the Expression of Ki67, RPS6, and Beta-Galactosidase Activity. *Int J Mol Sci*. 2021;22(6):3102.
73. Zhou S, Xi Y, Chen Y, Fu F, Yan W, Li M, et al. Low WIP1 Expression Accelerates Ovarian Aging by Promoting Follicular Atresia and Primordial Follicle Activation. *Cells*. 2022;11(23):3920.
74. Zlotnik A, Yoshie O. Chemokines: a new classification system and their role in immunity. *Immunity*. 2000;12(2):121–7.
75. Anisowicz A, Bardwell L, Sager R. Constitutive overexpression of a growth-regulated gene in transformed Chinese hamster and human cells. *Proc Natl Acad Sci U S A*. 1987;84(20):7188–92.
76. Korbecki J, Maruszewska A, Bosiacki M, Chlubek D, Baranowska-Bosiacka I. The Potential Importance of CXCL1 in the Physiological State and in Noncancer Diseases of the Cardiovascular System, Respiratory System and Skin. *Int J Mol Sci*. 2022;24(1):205.
77. Korbecki J, Bosiacki M, Barczak K, Łagocka R, Brodowska A, Chlubek D, et al. Involvement in Tumorigenesis and Clinical Significance of CXCL1 in Reproductive Cancers: Breast Cancer, Cervical Cancer, Endometrial Cancer, Ovarian Cancer and Prostate Cancer. *Int J Mol Sci*. 2023;24(8):7262.
78. Liu ZY, Zheng M, Li YM, Fan XY, Wang JC, Li ZC, et al. RIP3 promotes colitis-associated colorectal cancer by controlling tumor cell proliferation and CXCL1-induced immune suppression. *Theranostics*. 2019;9(12):3659–73.
79. Chen J, Fan ZX, Zhu DC, Guo YL, Ye K, Dai D, et al. Emerging Role of Dermal White Adipose Tissue in Modulating Hair Follicle Development During Aging. *Front Cell Dev Biol*. 2021;9: 728188.
80. Hasegawa M, Higashi K, Matsushita T, Hamaguchi Y, Saito K, Fujimoto M, et al. Dermokine inhibits ELR(+)CXC chemokine expression and delays early skin wound healing. *J Dermatol Sci*. 2013;70(1):34–41.
81. Feng M, Liu W, Ding J, Qiu Y, Chen Q. Sonic Hedgehog Induces Mesenchymal Stromal Cell Senescence-Associated Secretory Phenotype and Chondrocyte Apoptosis in Human Osteoarthritic Cartilage. *Front Cell Dev Biol*. 2021;9: 716610.

## Publisher's Note

Springer Nature remains neutral with regard to jurisdictional claims in published maps and institutional affiliations.